A R C H I V E O F M E C H A N I C A L E N G I N E E R I N G

VOL. LXI 2014 Number 2

10.2478/meceng-2014-0020

Key words: non-linear compliant mechanism, flexible multibody model, modal identification, manufacturing tolerances, exact constraint design

W. WIJMA [*], *S.E. BOER* [*], *R.G.K.M. AARTS* [*], *D.M. BROUWER* [*], *W.B.J. HAKVOORT* [*,**]

MODAL MEASUREMENTS AND MODEL CORRECTIONS OF A LARGE STROKE COMPLIANT MECHANISM

In modelling flexure based mechanisms, generally flexures are modelled perfectly aligned and nominal values are assumed for the dimensions. To test the validity of these assumptions for a two Degrees Of Freedom (DOF) large stroke compliant mechanism, eigenfrequency and mode shape measurements are compared to results obtained with a flexible multibody model. The mechanism consists of eleven cross flexures and seven interconnecting bodies. From the measurements 30% lower eigenfrequencies are observed than those obtained with the model. With a simplified model, it is demonstrated that these differences can be attributed to wrongly assumed leaf spring thickness and misalignment of the leaf springs in the cross flexures. These manufacturing tolerances thus significantly affect the behaviour of the two DOF mechanism, even though it was designed using the exact constraint design principle. This design principle avoids overconstraints to limit internal stresses due to manufacturing tolerances, yet this paper shows clearly that manufacturing imperfections can still result in significantly different dynamic behaviour.

1. Introduction

There is a growing demand from industry for high precision positioning mechanisms which can be used in vacuum environments and in the vicinity of UV light sources or electron beams. Conventional solutions like stages based on roller bearings suffer from hysteresis and wear. Furthermore they contaminate the vacuum due to evaporation of lubricants. Flexure based stages behave deterministic, are free of backlash and do not contaminate the vacuum environment [1-3]. Instead of distributed compliance, the stiffness should be lumped using flexure hinges, which maximizes out-of-plane stiffness, resistance to buckling and eigenfrequencies due to internal modes

[*] *Faculty of Engineering Technology, University of Twente, P.O. Box 217, 7500 AE Enschede, The Netherlands; E-mail: R.G.K.M.Aarts@utwente.nl*

[**] *DEMCON Advanced Mechatronics, Enschede, The Netherlands*

[3]. However misalignments in an overconstrained system can lead to unwanted changes in eigenfrequencies and stiffnesses [4, 5]. Hence to achieve deterministic behaviour, the principle of exact constraint design [6] should be taken into account. For monolithic designs, overconstraints in the out-of-plane direction are common [7, 8]. Due to high production accuracy, internal stresses remain limited. However, for large stroke applications, the allowable geometries of monolithic designs are too restrictive to achieve high supporting stiffnesses in a deflected state. For example advanced flexure hinges as in [9], which are non-monolithic, cannot be used to accomplish the motion. Hence, overconstraints should be avoided in non-monolithic mechanisms.

Brouwer et al. [10] designed and built a large stroke two DOF elastic mechanism using the exact constraint design method. The mechanism consists of eleven cross flexure hinges interconnected with links. Exact constraint design is realized by adding flexibility to the links in specific directions. The detailed design and preliminary eigenfrequency measurements of the mechanism are presented by Folkersma et al. [11]. The mechanism was exited and measured at only one location and thus mode shapes could not be obtained. In the undeflected state, higher eigenfrequencies were obtained with a finite element model than those resulting from the measurements. Because no mode shapes are available, it is hard to address the cause of the difference in eigenfrequencies.

For such insight more extensive measurements are required as we will show in the present paper. A nonlinear flexible multibody model is used, obtained with the SPACAR approach [12] and is compared to modal measurements in the full workspace of the mechanism. In maximizing the controller bandwidth, it is important that the first unwanted eigenfrequency and mode shape are predicted properly. Therefore the emphasis lays on comparing the first unwanted eigenfrequency and mode shape. To perform modal measurements, contactless measurements are favourable because these do not influence the dynamics. A laser Doppler vibrometer [13] appeared to be well-suited. Measurements are performed on a variety of locations on the two DOF mechanism, such that next to eigenfrequencies also mode shapes are available. Furthermore, the force direction of the excitation force needs to have a high repeatability, which is achieved by using a shaker for the excitation [14]. The differences between the measurement results and the model results are investigated by the use of a simplified model. The proposed modal measurement approach is used in this paper to analyze the two DOF mechanism, but it is more generally applicable for mechanical systems.

The mechanism and the model will be outlined first, secondly the modal measurement approach will be described. After that the results are presented.

Then a simplified model is used to interpret the results and finally some concluding remarks are given.

2. Two DOF compliant mechanism

The two DOF compliant mechanism is visualized in Fig. 1a. It consists of eleven hinges (labelled 1-11), connected by seven linkages (labelled *A*-*G*) and the end-effector (labelled *eff*). Translation of the end-effector in *x*- and *y*-direction are the degrees of freedom; the other degrees of freedom are suppressed. The encoders and actuators on arm *B* and *D* are used to control the rotation angles of these arms. The kinematic relation between the encoder readings and the end-effector position is used to position the end-effector in its workspace of 100×100 mm.

The two DOF mechanism consists of three loops as visualized in Fig. 1b. Each hinge allows rotation in one direction, which means that there are three overconstraints in each loop. This results in nine out-of-plane overconstraints, therefore nine compliances have to be added to obtain an exact constraint mechanism. Linkage C is designed such that it has three compliances. Furthermore three compliances are added by notch flexures close to the end-effector in arms *E*, *F* and *G* and three torsional compliances are added in those three arms [11].

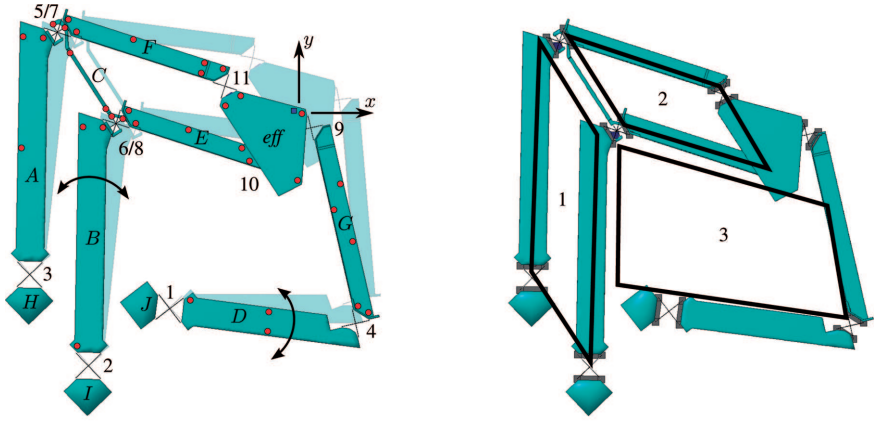

(a) Top view (b) Loops

Fig. 1. The two DOF mechanism: (a) Top view with measurement points; (b) The three closed loops

The cross flexures are made of Udeholm Stavax Supreme steel and are fabricated using the Electric Discharge Machining (EDM) technique. Linkage *C* together with cross flexures 7 and 8 are made out of one piece, also using the EDM technique and Udeholm Stavax Supreme steel. The other linkages are milled out of aluminium.

2.1. SPACAR model

The flexible multibody modelling approach implemented in the SPACAR software [12], is used to create a model. Beam elements are used to model the flexures. This element takes transverse shear and torsion-extension coupling into account [15]. The mass moments of inertia of the beam cross section are also considered. Furthermore, torsional stiffening due to constrained warping is included [9]. The linkages and the end-effector are modelled with the use of superelements [16]. These elements have 12 constrained modes to describe the deformations and have an equivalent mass and inertia distribution. Mass and inertia of bolts are included using nodal loads. The end-effector is positioned by applying a moment at arms B and D. The two DOF mechanism is mounted with base blocks H, I and J on a base plate. This plate is not included in the model and thus the three base blocks are fixed. Furthermore, gravity is taken into account.

2.2. Mode shapes

The first two eigenfrequencies are around 1.3 Hz and 2.6 Hz, and the accompanying mode shapes are movements in drive directions. This means these two modes can be excited and measured using the actuators and sensors of the two DOF mechanism. The stiffness properties of the manipulator in these driving directions do not change much throughout the operating range of the manipulator. In contrast, the supporting stiffness of deflected cross flexures is considerably lower compared to the undeflected configuration and hence the overall dynamic behaviour of the manipulator changes when the end-effector is moved. More specifically, the first few unwanted modes have movements perpendicular to the drive direction. The second unwanted mode shape for the neutral end-effector position is plotted as an example in Fig. 2.

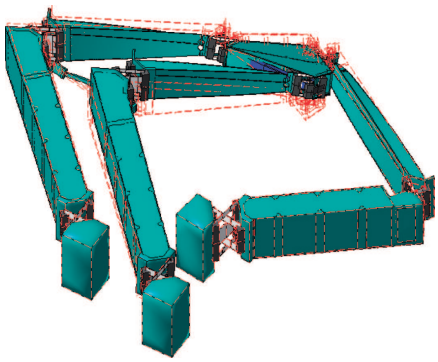

Fig. 2. Second unwanted mode from the model at neutral end-effector position at 121 Hz

Measurements in [11] show that this unwanted eigenfrequency is 105 Hz in the neutral configuration. However the model shows that this eigenfrequency is 121 Hz in the neutral configuration as can be seen later in Fig. 7.

3. Modal measurement approach

First the modal estimation method is outlined, which is followed by the measurement strategy. After that the experimental setup is described which is used to measure the vertical velocity of the mechanism at 35 locations, which are used as outputs. Each time the input force is measured at the same location, so that the phase information can be used to obtain mode shapes.

3.1. Modal estimation method

The modal estimation method consists of two parts, first a pole estimator is used which is the Least Squares Complex Frequency (LSCF) domain method [17]. The system poles are passed on to the residue estimator also called the Least Squares Frequency Domain (LSFD) method [18]. From the obtained residues the mode shapes can be estimated. A similar modal estimation method is implemented in [19], where characteristic loci are used to assess the stability of poles instead of the FRF estimates. However this is only possible for square multi-input multi-output (MIMO) systems, which is not the case in this paper. The method will be described briefly for a single-input multi-output (SIMO) case.

For the pole estimator the measured transfer functions between input and the j outputs are given as $H_j(\omega_f)$, where ω_f are the discrete frequencies. These j outputs are the 35 velocity measurements on the two DOF mechanism. The transfer functions are modelled with a common denominator model as

$$\hat{H}_j(\omega_f) = \frac{\sum_{k=1}^{n_n+1} \Omega_k(\omega_f) B_{jk}}{\sum_{k=1}^{n_n+1} \Omega_k(\omega_f) a_k} \tag{1}$$

where matrix $\boldsymbol{B}$ contains the real valued coefficients for the nominator polynomials of order n_n and vector $\boldsymbol{a}$ contains the real valued coefficients for the denominator polynomial also of order n_n. The discrete polynomial basis functions are given as

$$\Omega_k(\omega_f) = e^{-j\omega_f T_s(k-1)} \tag{2}$$

where T_s is the sampling time. After replacing the model $\hat{H}_j(\omega_f)$ in Eq. (1) by the measured FRF $H_j(\omega_f)$ and multiplying both sides with the denominator polynomial, it can be rewritten as

$$\sum_{k=1}^{n_n+1} \Omega_k(\omega_f) H_j(\omega_f) a_k - \sum_{k=1}^{n_n+1} \Omega_k(\omega_f) B_{jk} = e_j(\omega_f) \tag{3}$$

where $e_j(\omega_f)$ is the estimation error. Using a proper frequency dependent weighting function $w_j(\omega_f)$ ensures that multiple nearby poles are estimated properly [18]. The weighing function is given as

$$w_j(\omega_f) = \frac{\gamma_j^2(\omega_f)}{1 - \gamma_j^2(\omega_f)} \tag{4}$$

where $\gamma_j^2(\omega_f)$ is the coherence [20] which indicates the power transfer between input and the j^{th} output. When no weighting function is used, multiple nearby poles are estimated as one complex pole pair. With this weighting function included Eq. (3) can be rewritten as

$$\sum_{k=1}^{n_n+1} w_j(\omega_f) \Omega_k(\omega_f) H_j(\omega_f) a_k - \sum_{k=1}^{n_n+1} w_j(\omega_f) \Omega_k(\omega_f) B_{jk} = w_j(\omega_f) e_j(\omega_f) \tag{5}$$

This is the weighted linear least squares problem which has to be solved where the weighted error $w_j(\omega_f) e_j(\omega_f)$ is minimized, to obtain the parameters $\boldsymbol{a}$ and $\boldsymbol{B}$.

In [21] it is shown that when the last coefficient of $\boldsymbol{a}$ is fixed, the mathematical and system poles can be distinguished best. This principle is used to plot the stability charts. Then Eq. (5) is solved for increasing order of the denominator polynomial, while the last coefficient is fixed to one. Each time the order of the nominator polynomial is kept constant at the highest order. Furthermore the discrete poles are transformed to continuous poles. The stability charts can be used to judge which poles are system poles. The stability chart obtained from the measurements at the neutral end-effector position of the two DOF mechanism is plotted in Fig. 3a. The line is a summation of the absolute values of the measured transfer functions, which can be used as a reference. The dots indicate unstable poles i.e. poles with a positive real part, the crosses indicate stable poles i.e. poles with a negative real part. A system pole is identified if a stable pole occurs at the same frequency for a number of increasing orders and is denoted with a number in the stability chart. For reliable results the order n_n should be a bit higher

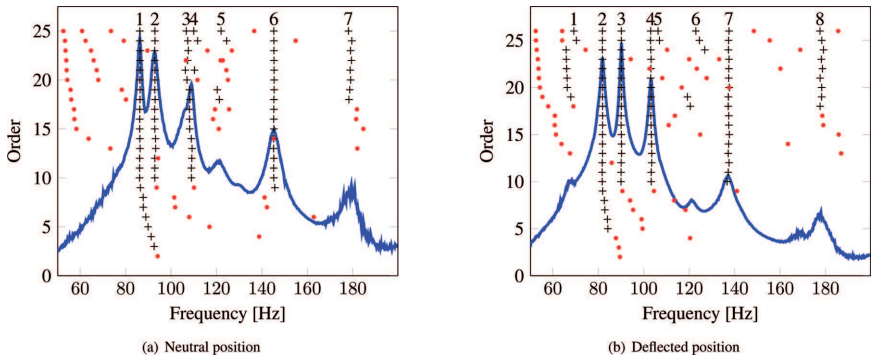

Fig. 3. Stability charts: (a) For neutral end-effector position; (b) At deviated end-effector position

than the real expected order of the system and the frequency range should be bounded to exclude low and high frequent noise and unwanted dynamics.

The continuous system poles are passed on to the residue estimator. For the case where the input is a force and the output is a velocity, the transfer functions are modelled in a pole residue form as

$$\hat{H}_j(\omega_f) = \sum_{k=1}^{n_p} \frac{i\omega_f R_{kj}}{(i\omega_f - \lambda_k)(i\omega_f - \bar{\lambda}_k)} \tag{6}$$

where λ_k and $\bar{\lambda}_k$ are the n_p complex system pole pairs obtained previously and R_{kj} is the residue of the k^{th} mode and the j^{th} output which are to be estimated. To give the model the same structure as the measurements, two residual terms are added [22]. Accounting for the fact that force to velocity transfer functions are obtained, this results in a $1/s$ term for lower suspension modes and an s term for higher truncated modes. Now the total model becomes

$$\hat{H}_j(\omega_f) = \sum_{k=1}^{n_p} \frac{i\omega_f R_{kj}}{(i\omega_f - \lambda_k)(i\omega_f - \bar{\lambda}_k)} + i\omega_f \bar{R}_{1j} + \frac{\bar{R}_{2j}}{i\omega_f} \tag{7}$$

where $\bar{R}_{1j}$ and $\bar{R}_{2j}$ are the additional residuals to be estimated. When again the model $\hat{H}_j(\omega_f)$ is replaced by the measured FRF $H_j(\omega_f)$ this becomes

$$\sum_{k=1}^{n_p} \frac{i\omega_f R_{kj}}{(i\omega_f - \lambda_k)(i\omega_f - \bar{\lambda}_k)} + i\omega_f \bar{R}_{1j} + \frac{\bar{R}_{2j}}{i\omega_f} - H_j(\omega_f) = e_j(\omega_f) \tag{8}$$

This linear least squares problem is solved by minimizing the error $e_j(\omega_f)$ to obtain the residues, which hold the amplitude information of the mode shapes. Proportional damping is assumed, so normal modes are obtained which means the residues are real-valued.

3.2. Measurement strategy

As mentioned before the unwanted mode shapes have mainly movements in out-of-plane direction. Therefore these modes are measured best when measuring and exciting in that direction. To obtain the required transfer functions, the velocity in vertical direction is measured at 35 positions on the two DOF mechanism, indicated by the red dots in Fig. 1a. The input force is measured at a fixed location indicated by the blue square in Fig. 1a. In selecting these measurement points, each part is considered independently. Three points are required to determine the out-of-plane position and the two orientations of the part. A fourth and fifth point are added to measure internal bending and torsion. For part F, a sixth point is added to measure the deflection of a notch-flexure.

The two DOF mechanism is analyzed for 65 equidistant end-effector positions on two arcs in the workspace as shown in Fig. 4. Both arcs cross at the neutral end-effector position. At the y-move arc the x actuator is standing still and at the x-move arc the y actuator is standing still. In each end-effector position, the velocity is measured in each of the 35 positions that are indicated in Fig. 1a and are at fixed relative positions on the respective links of the two DOF mechanism for each end-effector position. Because one of the two actuators is standing still at both arcs, a part of the mechanism is the same during each measurement on that arc. When a mode shape is mainly dependent of the dynamics in that part it is easier to link specific properties of the real mechanism to the model.

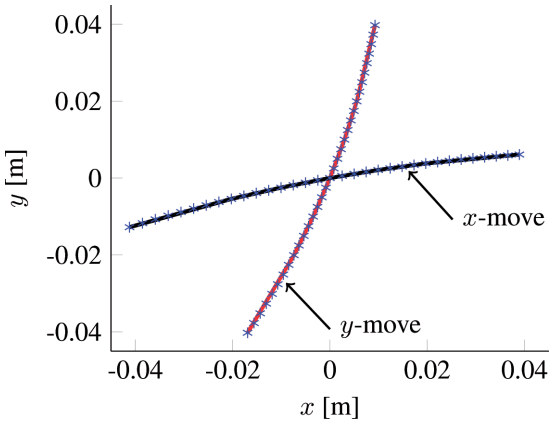

Fig. 4. End-effector positions over the workspace

Experiments are performed in the middle section of 80×80 mm of the total workspace of 100×100 mm. Outside this section the unwanted

eigenfrequencies of the mechanism are so low that the implemented controller cannot suppress the out-of-plane disturbances caused by the experiments.

3.3. Experimental setup

The measurement setup is shown in Fig. 5 and the equipment is listed in Tab. 1. A laser Doppler vibrometer mounted on a six DOF robot is used to measure the velocity in z-direction at 34 points on the two DOF mechanism. Retro-reflective tape is used to assure a high signal quality.

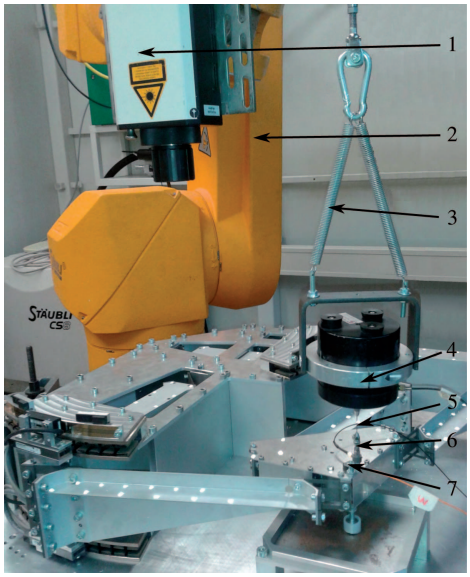

Fig. 5. Experimental measurement setup

Table 1.

Measurement equipment

No	Item	Type
1	Laser sensor head	Polytec OFV-303
2	Six DOF robot	Stäubli RX130
3	Suspension	–
4	Exciter	B&K 4810
5	Wire flexure	–
6	Force transducer	B&K 8203
7	Accelerometer	B&K 4517
-	Condition amplifier	B&K NEXUS
-	Power amplifier	B&K 2707
-	Digital signal processor	Siglab 4-channel model 20-42
-	Calibration exciter	B&K 4294
-	Computer	SigLab 3.28 and Matlab 6.5
-	Laser controller	Polytec OFV-3001

The two DOF mechanism is excited in the z-direction using a shaker which is suspended with a low frequent spring. A wire flexure ensures the excitation is directed the same for each measurement. The input force is measured using a force transducer. For each end-effector position the shaker was moved.

Underneath the shaker, a large area is not accessible for the laser Doppler vibrometer, so the motion is measured with an accelerometer that is located next to the force transducer. The acceleration signal is integrated to a velocity signal.

The accelerometer and force transducer signals are conditioned and processed together with the velocity data from the laser controller in a digital signal processor and transmitted to a computer, where the transfer functions and coherences are estimated using SigLab software. The bandwidth and measuring time are respectively 500 Hz and 65.6 s. Furthermore 20 averages are used with 50% overlap and a Hanning window was applied. As input a pseudo random noise excitation is used.

The combination of a laser Doppler vibrometer and the presented modal estimation method are firstly tested on a known monolithic object, from which it appeared that the method was well suited for an experimental modal analysis.

3.4. Validation experimental setup

3.4.1. Robot vibrations

The velocity is measured relatively from the Stäubli robot, therefore it is required that the Stäubli robot has a low vibration level. Measurements showed that the vibration level of the Stäubli robot was clearly acceptable.The velocity is measured relatively from the Stäubli robot, therefore it is required that the Stäubli robot has a low vibration level. Measurements showed that the vibration level of the Stäubli robot was clearly acceptable.

3.4.2. Suspension influence

The two DOF mechanism is mounted on 4 rubber blocks, which results in movements of the whole setup. Therefore, the baseplate motion is also measured at 7 distributed points for a number of end-effector positions. The ratio of the largest amplitude of the two DOF mechanism divided by the largest amplitude of the base plate is 88, 37, 10 and 13 respectively for the first four unwanted modes in the neutral configuration. This ensures that for the first two unwanted modes, the base plate is not moving significantly. However, the third and fourth unwanted mode have a large relative movement

of the baseplate. The baseplate is designed such that no internal modes are expected below 300 Hz.

3.4.3. Actuator influence

When the two DOF mechanism is analyzed for an end-effector position, the end-effector is kept in place using the actuators and sensors of the two DOF mechanism. A PD controller in combination with static force feed-forward is implemented. The influence of the actuators is tested by performing measurements with the end-effector at the neutral position having the motors powered and unpowered. It appeared that there was no significant difference between the unwanted eigenfrequencies and mode shapes of both measurements. In the other end-effector positions only the static contribution of the controller differs, the dynamic properties stay the same. Therefore it can be concluded that the actuators do not have a significant influence on the investigated dynamics of the two DOF mechanism for each end-effector position. Of course the actuators do affect the first two in-plane modes, but these are not of interest for the measurements in this paper.

3.4.4. Disturbances

A number of measurements showed eigenfrequencies around 70 Hz. In Fig. 3b the stability chart is plotted for the deviated end-effector position, $[x, y] = [0.0197, 0.0038]$ m, where an eigenfrequency is identified at 65 Hz. Extensive measurements by impacting the two DOF mechanism with a hammer and measuring the response with an inductive sensor at the end-effector in the z-direction, showed that the eigenfrequency was not present consistently. For example in Fig. 3a the eigenfrequency is not visible. Therefore it is concluded that it is an artefact of the measurement technique and these peaks are omitted in the measurement results.

4. Measurement and model results

4.1. Typical measurement

The measurement at the neutral end-effector position is used as an example to show the different steps in the measurements. The 35 transfer functions are analyzed by the pole estimator and the resulting stability chart is plotted in Fig. 3a. To get a proper result, order n_n had to be chosen in the range of 20 to 50 for each end-effector position, in this case the order was set to 25. The frequency range is set to 50 to 200 Hz, because with this range it is assured that the first unwanted eigenfrequency will be measured. As can be

seen seven system poles are identified in this case. Each peak is identified as an eigenfrequency and at 110 Hz two closely spaced eigenfrequencies are found.

The seven system poles are used in the residue estimator to estimate the mode shapes, from which a model of the system results. In Fig. 6 the measured transfer function from force to integrated accelerometer signal is plotted combined with its estimation. As can be seen the model is fitted well and only small differences are found.

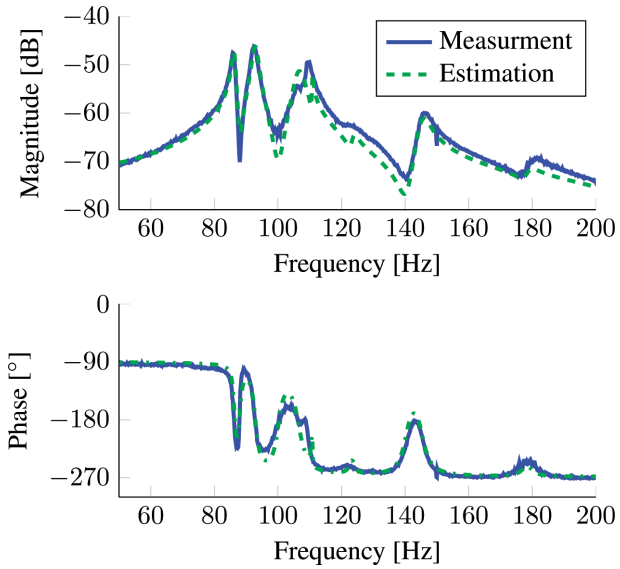

Fig. 6. A single measured transfer function with estimation at neutral end-effector

4.2. Results

In Fig. 7a the first four unwanted eigenfrequencies from the measurements (ω_{mi}) are compared to the first four unwanted eigenfrequencies from the model (ω_{si}) along the x-move arc from Fig. 4. In Fig. 7b the same comparison is made for the y-move arc. For the x-move eigenfrequencies, only the x coordinate of the end-effector location is used at the horizontal axis. Similarly, for the y-move arc only the y coordinate is used. In both cases the first two unwanted eigenfrequencies are plotted darker than the third and fourth eigenfrequencies, because only the first two unwanted eigenfrequencies will be discussed in the following text.

As can be seen in Fig. 7a two mode veering regions [23] occur at the ω_{s1} and ω_{s2} lines around $x = \pm 0.025$ m. In Fig. 7b the order of these two modes ω_{s1} and ω_{s2} changes as well around $y = \pm 0.025$ m.

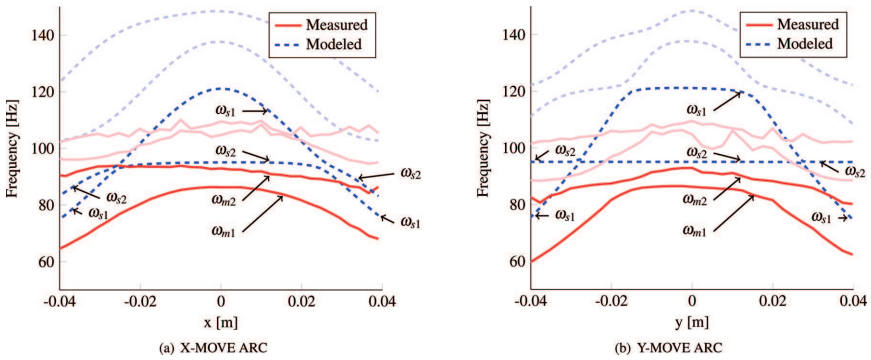

Fig. 7. First four unwanted eigenfrequencies obtained from measurements and model

Visual inspection shows that in both figures the eigenfrequencies denoted with ω_{s2} have a mode shape where mainly arm C is vibrating. This is the second mode shape in the measurements, which is plotted for the neutral end-effector position in Fig. 8. Therefore the ω_{s2} and the ω_{m2} lines have to be compared with each other. In a similar way the ω_{s1} and the ω_{m1} lines are linked to each other.

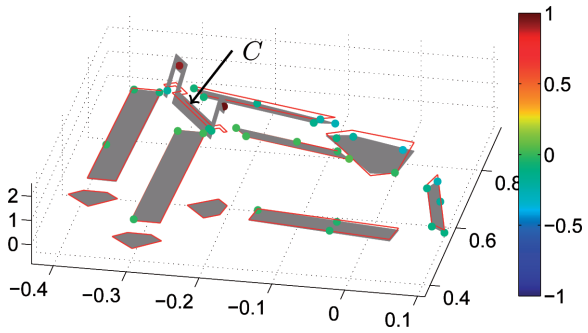

Fig. 8. Second unwanted mode from measurements at neutral end-effector position at 93 Hz

The differences between the ω_{m1} and the ω_{s1} lines are relatively and absolutely larger in the middle as at the edges. At the neutral end-effector position, the 86 Hz from the measurements is 30% lower than the 121 Hz from the model, whereas the shape is about the same. This means the model describes the general behaviour well, but the supporting stiffness of the cross flexures is much lower in the real mechanism compared to the model. The ω_{m2} and the ω_{s2} lines are closer to each other in both cases.

5. Differences between model and real setup

The measurements showed lower eigenfrequencies than the model, of which the differences between the ω_{m1} and the ω_{s1} lines are the most impor-

tant. The most likely causes of the differences are listed here with a short description.

- Leaf spring dimensions – The leaf springs are manufactured using the EDM process as mentioned before. During the EDM process, the wire will vibrate. The higher the part, the longer the wire and the larger the amplitude of vibration will be, which results in smaller dimensions. A thinner or smaller leaf spring means a lower supporting stiffness.
- Bending or torsion in the leaf springs - The leaf springs can be bent or twisted as drawn in Fig. 9, caused by internal stresses resulting from the EDM process and the leaf springs can be damaged during transport or assembly of the two DOF mechanism.
- Leaf spring mounting – The holes which hold the bolts and the dowel pins to mount the leaf springs can deviate from the location at the drawings. The flexibility of the leaf springs will allow the bolts to fit, but the resulting internal stresses in the cross flexures will lead to bent or twisted leaf springs.
- Mounting surface – If the surfaces at which the leaf springs are mounted do not have the proper angular values, the leaf springs will be mounted on a skew surface. And thus they will become bent or twisted.
- Closing a loop – The two DOF mechanism consist of three loops as can be seen in Fig. 1b. In one loop all mounting errors at the cross flexures and the gravity cause deviations. When the last flexure is mounted, the in-plane flexibility of the cross flexures and the local out-of-plane flexibility added for the exact constraint design will allow all bolts to fit. However, this causes the cross flexures to be mounted in a deflected state and its flexures will not be perfectly straight in the neutral end-effector position.

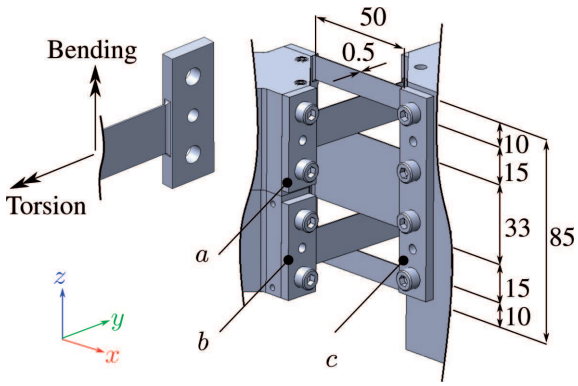

Fig. 9. Cross flexure dimensions in millimetres, bending and torsion visualized

The differences listed here all can have influence on the dynamic behaviour of the two DOF mechanism, but some of them have a larger impact than

others. Deviations in height and thickness of the leaf springs will all be in the order of tens of microns. With such a deviation only the thickness will have a significant influence. The other differences all come down to bent or twisted leaf springs. As can be seen in Fig. 9, a cross flexure consists of three parts: part *a*, *b* and *c*. The relatively small and thin parts *a* and *b* cause the most problems. They are easily damaged and they have to be mounted perfectly parallel with respect to each other to have no internal stresses. The three leaf springs in part *c* are perfectly aligned with respect to each other, because they are made out of one piece. To investigate the effects of the thickness, bending and twisting of the flexures on the dynamics of the two DOF mechanism, a simplified model is created.

5.1. Four link mechanism

To investigate the differences in eigenfrequencies a simplified model is made of loop 1 from Fig. 1b. This four link mechanism is created using SPACAR and the same modelling parameters are used as for the two DOF mechanism. The mass properties are adapted in such a way that the second eigenfrequency is comparable to the ω_{m1} and the ω_{s1} frequencies of the two DOF mechanism. The second eigenfrequency is used as a measure of performance. The two cross flexures at 2 and 3 are the same as in the complete model of the two DOF mechanism. A cross flexure with its dimensions is drawn in Fig. 9. The hinges at 1 and 4 only rotate around the z-axis. A model with two cross flexures is used such that the modelled imperfections in one cross flexure also affect the other cross flexure, which gives more representative results than when only one cross flexure is used.

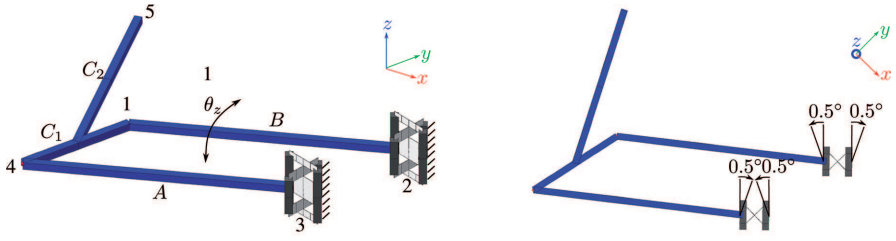

(a) Side top view ideal model (b) Top view model with rotated cross flexures

Fig. 10. Four link mode: (a) Undeflected configuration, (b) Top view of the model with rotated cross flexures

The flexures in both cross flexures are attached to each other with the use of rigid parts. At the right hand side the cross flexures are fixed. At the left hand side they are rigidly connected to rigid weightless links *A* and *B*. These links are connected by hinges to the rigid link C_1, which holds a distributed mass of 4.75 kg/m. The asymmetry of the two DOF mechanism

is reproduced by adding link C_2, which also holds a distributed mass of 4.75 kg/m. This link is connected rigidly to link C_1. Furthermore, a nodal mass of 1 kg is attached at point 5, which is at the centre of the end-effector.

By applying a moment around the z-axis at bar B, the four link mechanism can be actuated to angle θ_z. For the end-effector positions at which the two DOF mechanism is analyzed, the maximum deflection of the cross flexures is about $\pm 10^\circ$. Therefore, the four link model is analyzed in the range of -10° to $+10^\circ$ for θ_z.

The second eigenfrequency of the original four link model is plotted in Fig. 11. At the middle the second eigenfrequency is 102 Hz and at the sides it drops to 40 Hz and 53 Hz. The asymmetry in the graph is caused by the asymmetry in the model. To investigate the effect of torsion, torsional stress is introduced in parts a and b. However this showed no significant differences in the second eigenfrequency, therefore these results are omitted.

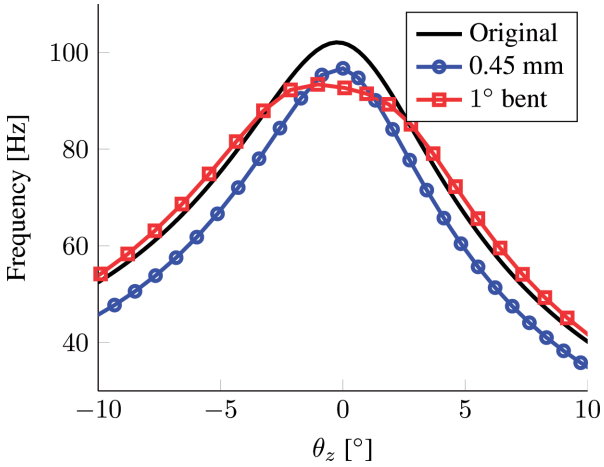

Fig. 11. Second eigenfrequency four link model

5.2. Leaf spring thickness

Measurements showed that the leaf spring thickness was 0.03 mm to 0.04 mm smaller than modelled. This means that the actual thickness is about 0.05 mm too small, when accounting for the roughness of the surface of the leaf springs. The second eigenfrequency using flexures with a thickness of 0.45 mm instead of 0.5 mm is plotted in Fig. 11. The difference compared to the original line is about 5 Hz over the whole angle of deflection.

5.3. Bending

Ideally the highest supporting stiffness of a cross flexure is in its neutral configuration. When the leaf springs are misaligned, all leaf springs are not in their neutral position in any mechanism configuration, which reduces the maximum supporting stiffness. With the manufacturing tolerances used, the highest supporting stiffness can be misaligned up to 1° from the neutral configuration of the two DOF mechanism. Therefore this is assumed as a worst case scenario.

The cross flexures are pre-stressed as in Fig. 10b. The four rigid connections are rotated 0.5° around the z-axis, which means both cross flexures are rotated 1° in opposite direction. Now the highest supporting stiffness of both cross flexures will be 1° out of its neutral configuration. The resulting second eigenfrequency is plotted in Fig. 11. A difference of 10 Hz is achieved with respect to the original four link model in the neutral configuration. Away from the neutral configuration, this difference decreases.

6. Discussion

The four link model is a suitable way to investigate the effects of construction errors on the two DOF mechanism. The bending effect has only influence in the middle of the stroke of the cross flexures of about 10%. The leaf spring thickness has a relative influence on the whole stroke of the cross flexures of about 5%. Both percentages do not add up to the 30% difference observed in Fig. 7. Note however that in the simplified four link model only two cross flexures are taken into account. When more cross flexures are included the difference is expected to be larger.

The thickness distribution of a leaf spring created by the EDM process, should be investigated more thoroughly to account for these manufacturing tolerances in the model. Furthermore it is demonstrated that a non-optimal design can be obtained, when the worst case scenario of manufacturing and alignment errors is not accounted for in the design.

7. Conclusion

In this paper modal measurements are presented on a large stroke two DOF cross flexure based positioning mechanism using a laser Doppler vibrometer positioned by a six DOF robot and a shaker as excitation. The modal measurement approach yielded a parametric model, that showed valuable insight in the dynamics of the two DOF mechanism. The measured force to velocity transfer functions showed position dependent eigenfrequencies

and mode shapes. The identified eigenfrequencies appear to be lower than predicted by a nonlinear flexible multibody model, created with the SPACAR software package. Still the qualitative behaviour was described well, in particular the drastic change in eigenfrequency away from the neutral end-effector position.

The cause of the differences are investigated using a simplified model, with a representative load case. It appears that a combination of manufacturing and alignment errors can lead to a decrease of the eigenfrequencies of the model with an amount comparable with the measurements. Therefore in designing non-monolithic flexure based mechanisms, the alignment errors should be minimized. For example, by minimizing the number of parts and use specially designed tools to properly align flexures with respect to each other. The remaining alignment and manufacturing errors should be accounted for in the modelling in order to obtain a reasonable prediction of dynamic properties such as eigenfrequencies.

The exact constraint design method is used in designing the two DOF mechanism, this method assures low internal stresses resulting from the manufacturing tolerances. However, these tolerances still have an influence on the performance of the mechanism. In general it can be stated that the importance of the tolerances should not be underestimated in designing and modelling compliant mechanisms.

Acknowledgment

This research is financially supported by the Dutch association Point-One, project MOV-ET PNE08006, by the Dutch Department of Economic Affairs, Agriculture and Innovation. The authors acknowledge the contribution from Bert Wolbert in providing the measurement equipment and giving technical support in setting up the experimental setup. Also the scripts with the modal estimation method provided by Dirk Tjepkjema where of a great help.

Manuscript received by Editorial Board, November 29, 2013;
final version, February 11, 2014.

REFERENCES

[1] Smith S.: *Flexures: Elements of Elastic Mechanisms.* Taylor & Francis, London, 2000.
[2] Howell L. L.: *Compliant Mechanisms.* Wiley, New York, 2001.
[3] Soemers H.J.M.R.: *Design Principles for Precision Mechanisms.* T-Pointprint, Enschede, 2010.
[4] Meijaard J.P., Brouwer D.M., Jonker J.B.: *Analytical and experimental investigation of a parallel leaf spring guidance.* Multibody Syst. Dyn. 23(1), pp. 77-97, 2010.

[5] Awtar S., Shimotsu K., Sen S.: *Elastic averaging in flexure mechanisms: A three-beam parallelogram flexure case study.* Journal of Mechanisms and Robotics 2(4), art. no. 041006, 2010.

[6] Blanding D.L.: *Exact Constraint: Machine Design Using Kinematic Principles.* ASME Press, New York, 1999.

[7] Moronuki N.: *Design of Silicon-Monolithic Flexure Stage with Selective Compliance.* JSME International Journal, Series C: Mechanical Systems, Machine Elements and Manufacturing, 47(1), pp. 111-116, 2010.

[8] Hao G., Kong X.: *A novel large-range XY compliant parallel manipulator with enhanced out-of-plane stiffness.* Journal of Mechanical Design, Transactions of the ASME 134(6), art. no. 061009, 2012.

[9] Wiersma D.H., Boer S.E., Aarts R.G.K.M., and Brouwer D.M.: *Design and performance optimization of large stroke spatial flexures.* Journal of Computational and Nonlinear Dynamics 9(1), 011016 (10 pages), 2013.

[10] Brouwer D.M., Folkersma K.G.P., Boer S.E., Aarts R.G.K.M.: *Exact Constraint Design of a Two-Degree of Freedom Flexure-Based Mechanism.* Journal of Mechanisms and Robotics 5(4), 041011 (10 pages), 2013.

[11] Folkersma K.G.P., Boer S.E., Brouwer D.M., Herder J.L., Soemers H.M.J.R.: *A 2-DOF Large Stroke Flexure Based Positioning Mechanism.* DETC2012-70377, International Design Engineering Technical Conferences & Computers and Information in Engineering Conference, Chicago, 2012.

[12] Jonker J.B., Meijaard J.P.: *SPACAR-computer program for dynamic analysis of flexible spatial mechanisms and manipulators.* In: Schiehlen W. (ed.) Multibody Systems Handbook, pp. 123-143. Springer, Berlin, 1990.

[13] Sracic M.W., Allen M.S., Sumali H.: *Identifying the Modal Properties of Nonlinear Structures Using Measured Free Response Time Histories from a Scanning Laser Doppler Vibrometer.* Conference Proceedings of the Society for Experimental Mechanics Series 3, pp. 269-286, 2012.

[14] Sujatha C.: *Vibration and acoustics : measurement and signal analysis.* New Delhi : Tata McGraw Hill Education Private Ltd., 2010.

[15] Jonker J.B., Meijaard J.P.: *A Finite Element Dynamic Analyses of Spatial Mechanisms with Flexible Links,* Computer Methods in Applied Mechanics and Engineering 76, pp. 17-40, 1989.

[16] Boer S., Aarts R., Meijaard J., Brouwer D., and Jonker J.: *A non-linear two-node superelement for use in flexible multibody systems.* Multibody System Dynamics 31 (4), pp. 405-431. DOI: 10.1007/s11044-013-9373-8.

[17] van der Auweraer H., Guillaume P., Verboven P., Vanlanduit S.: *Application of a Fast-Stabilizing Frequency Domain Parameter Estimation Method.* Journal of Dynamic Systems, Measurement and Control, 123(4), pp. 651-658, 2001.

[18] Verboven P.: *Frequency-Domain System Identification for Modal Analysis.* PhD thesis, Vrije Universiteit Brussel, Brussel, 2002.

[19] Tjepkema D.: *Active hard mount vibration isolation for precision equipment,* 9789036534185, University of Twente, November, 2, 2012. DOI: 10.3990/1.9789036534185.

[20] Siglab S.: *Estimating Transfer Functions with SigLab.* DSP Technology Inc, United States of America, 1994.

[21] Cauberghe B., Guillaume P., Verboven P., Vanlanduit E., Parloo E.: *On the influence of the parameter constraint on the stability of the poles and the discrimination capabilities of the stabilization diagrams.* Mechanical Systems and Signal Processing 19 (5), pp. 989-1014, 2005.

[22] Balmès E.: *Frequency Domain Identification of Structural Dynamics Using the Pole/Residue Parameterization.* IMAC, 28, pp. 540-546, 1995.

[23] Bonisoli E., Delprete C., Esposito M., Mottershead J.E.: *Structural Dynamics with Coincident Eigenvalues: Modelling and Testing.* Conference Proceedings of the Society for Experimental Mechanics Series 3, pp. 325-337, 2011.

Pomiary modalne i korekcje modelu mechanizmu podatnego o długim suwie

S t r e s z c z e n i e

W modelowaniu mechanizmów opartych na ugięciach na ogół zakłada się, że ugięcia są doskonale wyrównane liniowo i przyjmuje nominalne wartości wymiarów. By sprawdzić zasadność tych założeń dla podatnego mechanizmu o długim suwie i dwu stopniach swobody porównano wyniki pomiarów wartości własnych i kształtu modów z wynikami otrzymanymi na podstawie sprężystego modelu wielu ciał. W mechanizmie występuje jedenaście poprzecznych elementów giętych i siedem wzajemnie powiązanych ciał. Wartości własne wyznaczone pomiarowo były o 30% mniejsze od obliczonych na podstawie modelu. Można wykazać, że w uproszczonym modelu różnice te należy przypisać wadliwie przyjętej grubości sprężyny płytkowej i złemu wyrównaniu sprężyn w poprzecznych elementach sprężystych. Jak stąd wynika, tolerancje wykonania silnie wpływają na zachowanie mechanizmu o dwu stopniach swobody, mimo że był on zaprojektowany przy zachowaniu zasady ścisłych więzów. Taką zasadę projektowania stosuje się, by zapobiec tworzeniu więzów nadmiarowych i ograniczyć naprężenia wewnętrzne powstałe w wyniku niedokładności wykonania. Niemniej, w artykule pokazano wyraźnie, że niedokładności wykonania mogą wciąż powodować istotne zmiany we właściwościach dynamicznych mechanizmu.